Determination of enhancement ratios of HCOOH relative to CO in biomass burning plumes by the Infrared Atmospheric Sounding Interferometer (IASI)

Matthieu Pommier, Cathy Clerbaux, Pierre-François Coheur

Atmos. Chem. Phys., 17, 11089–11105, 2017
https://doi.org/10.5194/acp-17-11089-2017

Atmospheric Chemistry and Physics
Open Access
EGU

Determination of enhancement ratios of HCOOH relative to CO in biomass burning plumes by the Infrared Atmospheric Sounding Interferometer (IASI)

Matthieu Pommier[1,a], **Cathy Clerbaux**[1,2], **and Pierre-Francois Coheur**[2]

[1]LATMOS/IPSL, UPMC Univ. Paris 06 Sorbonne Universités, UVSQ, CNRS, Paris, France
[2]Spectroscopie de l'Atmosphère, Chimie Quantique et Photophysique, Université Libre de Bruxelles (ULB), Brussels, Belgium
[a]now at: Norwegian Meteorological Institute, Oslo, Norway

Correspondence to: Matthieu Pommier (matthieup@met.no)

Received: 8 February 2017 – Discussion started: 28 February 2017
Revised: 9 August 2017 – Accepted: 22 August 2017 – Published: 20 September 2017

Abstract. Formic acid (HCOOH) concentrations are often underestimated by models, and its chemistry is highly uncertain. HCOOH is, however, among the most abundant atmospheric volatile organic compounds, and it is potentially responsible for rain acidity in remote areas. HCOOH data from the Infrared Atmospheric Sounding Interferometer (IASI) are analyzed from 2008 to 2014 to estimate enhancement ratios from biomass burning emissions over seven regions. Fire-affected HCOOH and CO total columns are defined by combining total columns from IASI, geographic location of the fires from Moderate Resolution Imaging Spectroradiometer (MODIS), and the surface wind speed field from the European Centre for Medium-Range Weather Forecasts (ECMWF). Robust correlations are found between these fire-affected HCOOH and CO total columns over the selected biomass burning regions, allowing the calculation of enhancement ratios equal to $7.30 \times 10^{-3} \pm 0.08 \times 10^{-3}$ mol mol^{-1} over Amazonia (AMA), $11.10 \times 10^{-3} \pm 1.37 \times 10^{-3}$ mol mol^{-1} over Australia (AUS), $6.80 \times 10^{-3} \pm 0.44 \times 10^{-3}$ mol mol^{-1} over India (IND), $5.80 \times 10^{-3} \pm 0.15 \times 10^{-3}$ mol mol^{-1} over Southeast Asia (SEA), $4.00 \times 10^{-3} \pm 0.19 \times 10^{-3}$ mol mol^{-1} over northern Africa (NAF), $5.00 \times 10^{-3} \pm 0.13 \times 10^{-3}$ mol mol^{-1} over southern Africa (SAF), and $4.40 \times 10^{-3} \pm 0.09 \times 10^{-3}$ mol mol^{-1} over Siberia (SIB), in a fair agreement with previous studies. In comparison with referenced emission ratios, it is also shown that the selected agricultural burning plumes captured by IASI over India and Southeast Asia correspond to recent plumes where the chemistry or the sink does not occur. An additional classification of the enhancement ratios by type of fuel burned is also provided, showing a diverse origin of the plumes sampled by IASI, especially over Amazonia and Siberia. The variability in the enhancement ratios by biome over the different regions show that the levels of HCOOH and CO do not only depend on the fuel types.

1 Introduction

Formic acid (HCOOH) is one of the most abundant carboxylic acids present in the atmosphere. HCOOH is mainly removed from the troposphere through wet and dry deposition, and to a lesser extent by the OH radical. It is a relatively short-lived species with an average lifetime in the troposphere of 3–4 days (Paulot et al., 2011; Stavrakou et al., 2012). HCOOH contributes a large fraction to acidity in precipitation in remote areas (e.g., Andreae et al., 1988).

HCOOH is mainly a secondary product from other organic precursors. The largest global source of HCOOH is biogenic and follows the emissions of isoprene, monoterpenes, other terminal alkenes (e.g., Neeb et al., 1997; Lee et al., 2006; Paulot et al., 2011), alkynes (Hatakeyama et al., 1986; Bohn et al., 1996), and acetaldehyde (Andrews et al., 2012; Clubb et al., 2012). There are also small direct emissions by vegetation (Keene and Galloway, 1984, 1988; Gabriel et al., 1999) and biomass burning (e.g., Goode et al., 2000). Other

studies highlighted the existence of other sources, such as from ants (Graedel and Eisner, 1988), dry savanna soils (Sanhueza and Andreae, 1991), motor vehicles (Kawamura et al., 1985; Grosjean, 1989), abiological formation on rock surfaces (Ohta et al., 2000), and cloud processing (Chameides and Davis, 1983). Their contributions are very uncertain and most are probably minor.

More generally there are still large uncertainties on the sources and sinks of HCOOH, and on the relative contribution of anthropogenic and natural sources, despite the fact that recent progress has been made possible by using the synergy between atmospheric models and satellite data (e.g., Stavrakou et al., 2012; Chaliyakunnel et al., 2016). These uncertainties have an impact on our understanding of the HCOOH tropospheric chemistry, as on the oxidizing capacity of the atmosphere (i.e., the chemistry of OH in cloud water – Jacob, 1986; the heterogeneous oxidation of organic aerosols – Paulot et al., 2011) or the origin of the acid rains. One of the large uncertainties in the HCOOH tropospheric budget seems to be the underestimation of the emissions from forest fires, as recently suggested by Stavrakou et al. (2012), Cady-Pereira et al. (2014), and Chaliyakunnel et al. (2016).

One way to estimate the atmospheric emissions of pyrogenic species is the use of emission factors. The emission factors are often obtained from ground and airborne measurements or from small fires burned under controlled laboratory conditions. The emission factors can also be derived from enhancement ratios of the target species relative to a reference species, which is often carbon monoxide (CO) or carbon dioxide (CO_2) due to their long lifetime (e.g., Hurst et al., 1994) and are based on the characteristic of the combustible and hence depend on the type of biomass burning. However, the difference between an emission ratio and an enhancement ratio is that emission ratios are calculated from measurements at the time of emission and enhancement ratios are related to the ongoing chemistry. To correctly convert these enhancement ratios to emission ratios, the decay of the chemical species needs to be taken into account or assumptions need to be made, suggesting that the enhancement ratios are equivalent to emission ratios, hence measured at the source and not impacted by chemistry.

Compilations of numerous enhancement ratios, emission ratios, and emission factors for several trace gases from measurements at various locations worldwide are published regularly (e.g., Akagi et al., 2011) in order to facilitate their use in chemistry transport models.

There has been a recent interest in calculating enhancement ratios and emission factors from satellite data (e.g., Rinsland et al., 2007; Coheur et al., 2009; Tereszchuk et al., 2011). The above difficulty of inferring emission factors using the satellite observations comes from the fact that these observations are indeed typically made in the free–upper troposphere and further downwind of the fires. The fact that satellites mainly probe transported plumes where chemistry modifies the original composition explains why the use of the enhancement ratio is more relevant than emission ratio.

Only a few papers have reported on the use of satellite retrievals to study tropospheric HCOOH, including the nadir-viewing Infrared Atmospheric Sounding Interferometer (IASI; e.g., Razavi et al., 2011; Stavrakou et al., 2012; R'Honi et al., 2013; Pommier et al., 2016) and Tropospheric Emission Spectrometer (TES; e.g., Cady-Pereira et al., 2014; Chaliyakunnel et al., 2016). Other studies have used the solar occultation Atmospheric Chemistry Experiment–Fourier Transform Spectrometer (ACE-FTS), which measures the atmospheric composition in the upper troposphere (e.g., Rinsland et al., 2006; Gonzalez Abad et al., 2009; Tereszchuk et al., 2011, 2013), and the Michelson Interferometer for Passive Atmospheric Sounding (MIPAS) limb instrument, which is sensitive to around 10 km (Grutter et al., 2010).

These infrared (IR) sounders have limited vertical sensitivity as compared to ground-based or airborne measurements, but their spatial coverage represents a major advantage, which allows observation of remote regions which are sparsely studied by field measurements, like the biomass burning regions.

This work aims to provide a list of enhancement ratios of HCOOH relative to CO over several biomass burning regions. For this, we analyzed 7 years of IASI measurements, between 2008 and 2014. Section 2 describes the IASI satellite mission and the retrieval characteristics for the CO and the HCOOH total columns. Section 3 presents the fire product used from the Moderate Resolution Imaging Spectroradiometer (MODIS) to identify the fire locations. Section 4 details the methodology used to identify of the IASI fire-affected observations. In Sect. 5 we describe and analyze the enhancement ratios obtained from the IASI measurements, including an analysis of these ratios by type of fuel burned, and we compare these values to those available in the literature. Finally, the conclusions are presented in Sect. 6.

2 HCOOH and CO columns from IASI

2.1 The IASI mission

IASI is a nadir-viewing Fourier transform spectrometer. Two models are currently in orbit. The first model (IASI-A) was launched onboard the Meteorological Operational Satellite (METOP)-A platform in October 2006. The second instrument was launched in September 2012 onboard METOP-B. Owing to its wide swath, IASI delivers near-global coverage twice a day with observation at around 09:30 and 21:30 local time. Each atmospheric view is composed of 2×2 circular pixels with a 12 km footprint diameter, spaced out by 50 km at nadir. IASI measures in the thermal infrared part of the spectrum, between 645 and 2760 cm^{-1}. It records radiance from the Earth's surface and the atmosphere with an apodized spectral resolution of 0.5 cm^{-1}, spectrally sampled

at 0.25 cm^{-1}. IASI has a wavenumber-dependent radiometric noise ranging from 0.1 to 0.4 K for a reference blackbody at 280 K (Clerbaux et al., 2009), and more specifically around 0.15 K for HCOOH and 0.20 K for the CO spectral ranges ($\sim 1105\,cm^{-1}$ and $\sim 2150\,cm^{-1}$, respectively).

The HCOOH and CO columns from IASI are used hereafter to determine the enhancement ratios of HCOOH. CO is chosen as reference due to its longer tropospheric lifetime (a few weeks to a few months, depending on latitude and time of year) as compared to HCOOH. In our study we use CO as the reference and not CO_2, since variations in CO_2 concentration are difficult to measure with sufficient accuracy from IASI (Crevoisier et al., 2009).

2.2 The CO retrieval characteristics

The CO concentrations are retrieved from IASI using the FORLI-CO software (Hurtmans et al., 2012), which uses an optimal estimation method based on Rodgers (2000). The spectral range used for the retrieval is between 2143 and 2181.25 cm^{-1}. The CO total columns have been validated for different locations and atmospheric conditions (e.g., De Wachter et al., 2012; Kerzenmacher et al., 2012), and the comparisons with other data have shown good overall agreement, even if some discrepancies were found within CO-enriched plumes (reaching 12 % over the Arctic in summer, see Pommier et al., 2010; and reaching 17 % in comparison with other IR sounders, see George et al., 2009). These data were also used previously to study biomass burning plumes (e.g., Turquety et al., 2009; Pommier et al., 2010; Krol et al., 2013; Whitburn et al., 2015).

In order to keep only the most reliable retrievals, the selected data used have a root-mean-square error lower than $2.7 \times 10^{-9}\,W\,(cm^2\,cm^{-1}\,sr)^{-1}$ and a bias ranging between -0.15 and 0.25×10^{-9} as recommended in Hurtmans et al. (2012).

2.3 The HCOOH retrieval characteristics

The retrieval is based on the determination of the brightness temperature difference (ΔT_b) between spectral channels with and without the signature of HCOOH. The reference channels used for the calculation of ΔT_b were chosen on both sides of the HCOOH Q-branch ($1105\,cm^{-1}$), i.e., at 1103.0 and 1109.0 cm^{-1}. These ΔT_b were converted into total columns of HCOOH using conversion factors compiled in lookup tables. This simple and efficient retrieval method is described in more detail in Pommier et al. (2016).

As shown in Pommier et al. (2016), the vertical sensitivity of the IASI HCOOH total column ranges between 1 and 6 km. That study also showed that large HCOOH total columns were detected over biomass burning regions (e.g., Africa, Siberia) even if the largest values were found to be underestimated. This underestimation, which is less than 35 % for the columns smaller than $2.5 \times 10^{16}\,molec\,cm^{-2}$ (Pommier et al., 2016), will affect the enhancement ratios calculated in this work.

On the other hand, a large overestimation of the IASI HCOOH columns was shown in comparison with ground-based FTIR (Fourier transform infrared) measurements. This overestimation was larger for background columns (expected to reach 80 % for a column close to $0.3 \times 10^{16}\,molec\,cm^{-2}$), which can also impact our enhancement ratios.

3 MODIS

To identify the fire locations (hotspots), the fire product from MODIS onboard the polar-orbiting sun-synchronous NASA Terra and Aqua satellites (Justice et al., 2002; Giglio et al., 2006) are used. The Terra and Aqua satellites' equatorial overpass times are $\sim$ 10:30 and 22:30 and $\sim$ 01:30 and 13:30 local time, respectively. Fire pixels are 1 km × 1 km in size at nadir.

For this work, we more specifically use the Global Monthly Fire Location Product (MCD14ML, Level 2, Collection 5) developed by the University of Maryland (https://earthdata.nasa.gov/data/near-real-time-data/firms/active-fire-data#tab-content-6) which, for each detected fire pixel, includes the geographic location of the fire, the fire radiative power (FRP), the confidence in detection, and the acquisition date and time. The FRP provides a measure of fire intensity that is linked to the fire fuel consumption rate (e.g., Wooster et al., 2005). Only data presenting a high confidence percentage are used, i.e., higher than or equal to 80 % as recommended in the MODIS user's guide (Giglio, 2013).

To characterize each MODIS hotspot by the type of fuel burned, the Global Mosaics of the standard MODIS land-cover-type data product (MCD12Q1) in the IGBP land-cover-type classification (Friedl et al., 2010; Channan et al., 2014) with a 0.5° × 0.5° horizontal resolution has also been used (http://glcf.umd.edu/data/lc/). As the annual variability in this product is limited (not shown) and since the period available (from 2001 to 2012) does not fully match the period of the IASI mission, only the data for 2012 have been used. Whitburn et al. (2017) have also used this MCD12Q1 product to determine their IASI-derived NH_3 enhancement ratios by vegetation types.

4 Identifying fire-affected IASI observations

4.1 The selected areas

The determination of the biomass burning regions is based on the MODIS fire product. Figure 1 highlights the main areas that contributed to the biomass burning for the period between 2008 and 2014. Seven regions were selected for this work: Amazonia (AMA; 5–15° S, 40–60° W), corresponding mainly to the Brazilian Cerrado; Australia (AUS;

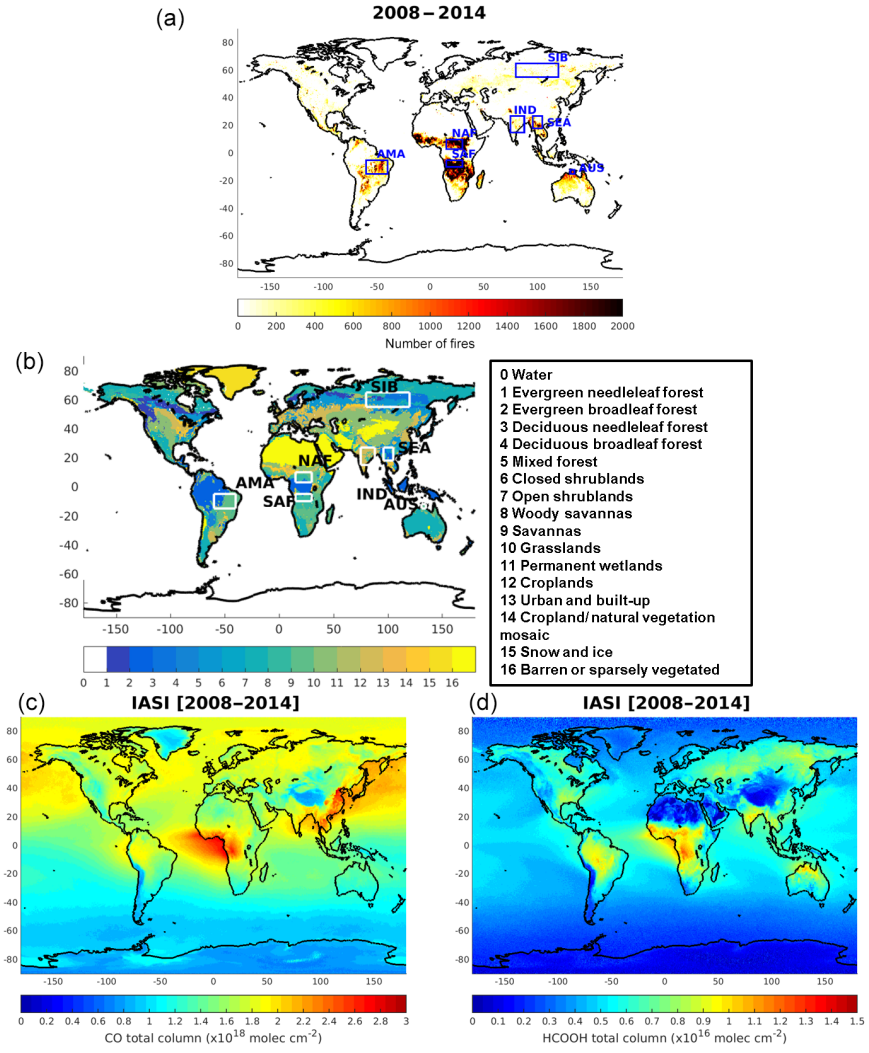

Figure 1. (a) Number of MODIS fire hotspots with a confidence percentage higher than or equal to 80 %, averaged on a 0.5° × 0.5° grid, for the period between 2008 and 2014. The blue boxes are the regions studied in this work. **(b)** Classification of the land cover type from MODIS on the same grid and highlighting the studied regions in white. Each number corresponds to the type of vegetation. Only the data between 64° S and 84° N are available. The IASI CO total column distribution **(c)** and the IASI HCOOH total column distribution **(d)**, averaged between 2008 and 2014 and on the same grid.

12–15° S, 131–135° E); northern Africa (NAF; 3–10° N, 15–30° E); southern Africa (SAF; 5–10° S, 15–30° E); Southeast Asia (SEA; 18–27° N, 96–105° E); India (IND; 15–27° N, 75–88° E); and Siberia (SIB; 55–65° N, 80–120° E). Among these regions, India and Siberia do not represent the most active regions in terms of number of fires. It seemed, however, important to also investigate them. One first reason for this is that Pommier et al. (2016) showed a misrepresentation of the fire emissions of HCOOH over India. Secondly, India also encounters excess acidity in rainwater, which could be partly attributed to biomass burning (e.g., Bisht et al., 2014). Concerning Siberia, this region and the surrounding areas experienced intense fires over some years, such as during the summer 2010 (Pommier et al., 2016; and R'Honi et al., 2013, for the region close to Moscow). The classification of the vegetation from the MODIS product has also been used for a detailed analysis of the enhancement ratios for these regions (Fig. 1).

4.2 The IASI data used

For this work, both the daytime and nighttime IASI data were used. We have verified that using only the daytime retrievals did not change the results. Figure 2 presents the time series of the monthly mean for the HCOOH and CO total columns over the seven selected regions. The number of fires and their FRP are also indicated. The variation in the total columns of HCOOH and CO matches relatively well with the variation

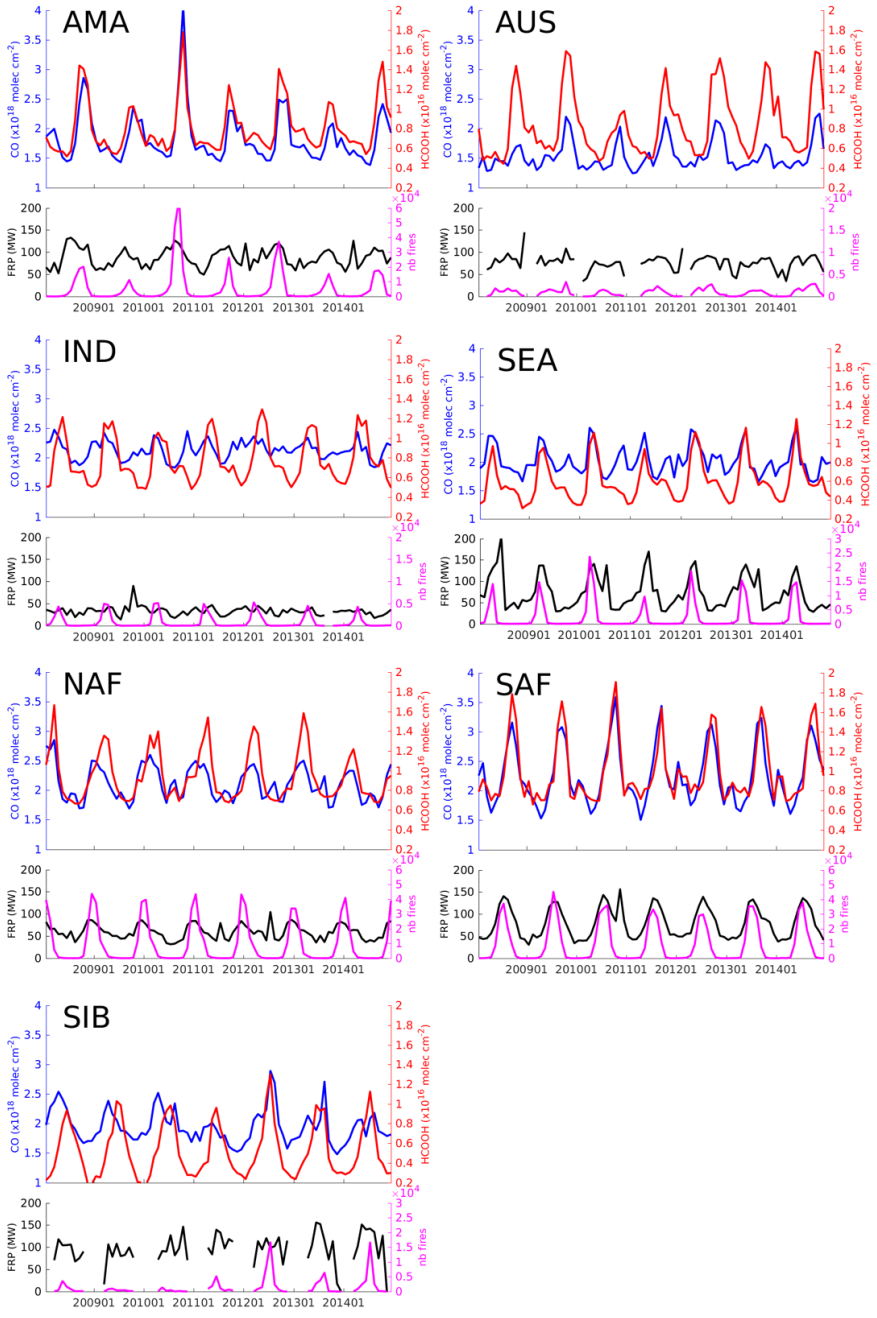

Figure 2. Time series from 2008 to 2014 of the monthly means of IASI CO (blue) and HCOOH (red) total columns in 10^{18} molec cm^{-2} and in 10^{16} molec cm^{-2}, respectively; FRP (black) in megawatts (MW); and the number of fires (nb fires, magenta) from MODIS over the seven regions (AMA, Amazonia; AUS, Australia; IND, India; SEA, Southeast Asia; NAF, northern Africa; SAF, southern Africa; SIB, Siberia).

of the number of fires. It is also worth noting that these variations in the total columns do not depend on the intensity of the fires as shown by Fig. 2 and by the scatterplots with the values characterizing each fire as described below (not shown).

The monthly HCOOH and CO total columns are found to be highly correlated over the selected biomass burning regions (correlation coefficient, r, from 0.75 to 0.91), except over India ($r = 0.34$) and Siberia ($r = 0.58$). Over both regions, the impact of sources other than biomass burning is thus not negligible. Over India, the CO budget is influenced by long-range transport (e.g., Srinivas et al., 2016) and the anthropogenic emissions also have a large impact (e.g., Ohara et al., 2007). This could explain why the variation in CO does not perfectly follow the variation in the number of fires and why the difference between the background level

and the CO peaks is less marked than for the HCOOH. Over Siberia, a temporal shift between the highest peaks for CO and for HCOOH is noticed for some years, such as for 2009, 2010, and 2011. For these years, the variation in CO does not follow the variation in the number of fires. The large region selected over Siberia is known to also be impacted by CO-enriched plumes transported from other regions, such as polluted air masses from China (e.g., Paris et al., 2008) or from Europe (e.g., Pochanart et al., 2003). These external influences interfere with the CO plumes originating from forest fires measured over this region.

Despite the overall good match between the number of fires and the variation in HCOOH and CO, we are not certain that HCOOH and the CO were emitted solely by fires, and the discrimination between a natural and an anthropogenic origin for each compound is challenging. This assessment is particularly obvious for IND and SIB. To isolate the HCOOH and CO signals measured by IASI, potentially emitted by a fire, we decided to only use the data in the vicinity of each MODIS hotspot. To do so, we co-located the IASI data at 50 km around each MODIS pixel and between 0 and 5 h from the time registered by MODIS for each detected fire, so that each MODIS pixel is associated with a mean value of HCOOH and CO total columns from IASI.

With these co-location criteria, good correlation coefficients, calculated by linear-least-squares fitting, are found between the HCOOH and CO total columns as shown in Table 1 (upper row). The smaller correlation coefficients, i.e., less than 0.7, are found for India, Australia, Siberia, and northern Africa. It is also important to note that the HCOOH and CO columns are better correlated for India and Siberia compared to the monthly time series shown in Fig. 2. The three other regions present a large correlation, around 0.8. The high correlation suggests that IASI sampled the same biomass burning air mass for these compounds.

4.3 Importance of the meteorological conditions

As shown in earlier studies, the wind speed can have a large influence on the detection of tropospheric plumes of trace gases from space (e.g., NO_2: Beirle et al., 2011; CO: Pommier et al., 2013; SO_2: Fioletov et al., 2015). We have chosen to assign a surface wind speed value for each MODIS hotspot. These meteorological fields were taken from the ECMWF (European Centre for Medium-Range Weather Forecasts) reanalysis data (http://apps.ecmwf.int/datasets/data/interim-full-daily/levtype=sfc/; Dee et al., 2011). The horizontal resolution of these fields is 0.125° on longitude and latitude with a 6 h time step. As shown in Fig. 3, the three regions where the HCOOH : CO correlations are found to be high (r close to 0.8) correspond to the regions where the surface wind speed was lower, i.e., for AMA, SEA, and SAF. IND also has a low mean and median surface wind speed, but the distribution of this surface wind speed over IND is more spread out than for AMA, SEA, and SAF. It is

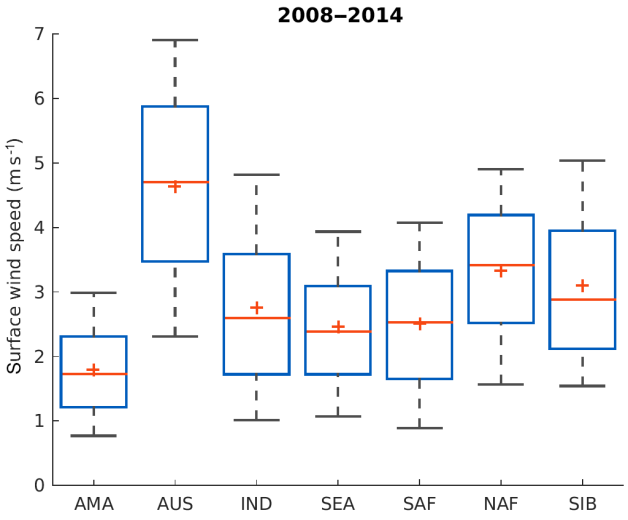

Figure 3. Box and whisker plots showing the mean (red central cross), median (red central line), and 25th and 75th percentiles (blue box edges) of surface wind speed for each MODIS hotspot over the studied regions (AMA = Amazonia, AUS = Australia, IND = India, SEA = Southeast Asia, NAF = northern Africa, SAF = southern Africa, SIB = Siberia). The whiskers encompass values from the $25\text{th} - 1.5 \times (75\text{th} - 25\text{th})$ to the $75\text{th} + 1.5 \times (75\text{th} - 25\text{th})$ percentiles. This range of values corresponds to approximately 99.3 % coverage if the data are normally distributed.

also noteworthy that the IND and SEA regions are both characterized by higher wind speed at higher altitudes, i.e., for the pressure levels 650 and 450 hPa (not shown). This shows that the wind speed at higher altitudes has a lower influence on our correlations than the surface wind. When filtering out the data associated with a large surface wind (higher than $1.44\,\mathrm{m\,s^{-1}}$), new correlations between the HCOOH and the CO total columns from IASI are calculated (Table 1 – lower row). This value of $1.44\,\mathrm{m\,s^{-1}}$ for the surface wind speed corresponds to the 25th percentile of the distribution of the three regions characterized by the lowest surface wind speed (Fig. 3).

The correlation coefficients, shown on the scatterplots in Fig. 4 and summarized in Table 1 (lower row), increase for all regions except over NAF, where the coefficient is found to be slightly lower than the previous correlation (Table 1 – upper row). The correlation coefficient is significantly improved over IND and SIB (Table 1 – lower row). These results confirm a robust correlation between the HCOOH and the CO total columns measured by IASI in the vicinity of each MODIS fire location.

Table 1. Upper row: correlation coefficients between the HCOOH total columns and the CO total columns measured by IASI for the period between 2008 and 2014 over the seven studied regions. Lower row: as upper row but with only MODIS fire hotspot having a surface wind speed lower than 1.44 m s^{-1}. Each IASI datapoint is selected in an area of 50 km around the MODIS fire hotspot and up to 5 h after the time recorded for each fire. The number of fires characterized by HCOOH and CO total columns is given in parenthesis.

	AMA	AUS	IND	SEA	SAF	NAF	SIB
r	0.78 (13 342)	0.63 (1525)	0.53 (1641)	0.84 (1865)	0.78 (12 227)	0.58 (21 139)	0.65 (22 353)
	0.79 (4580)	0.65 (93)	0.65 (340)	0.86 (528)	0.80 (895)	0.53 (1095)	0.72 (2097)

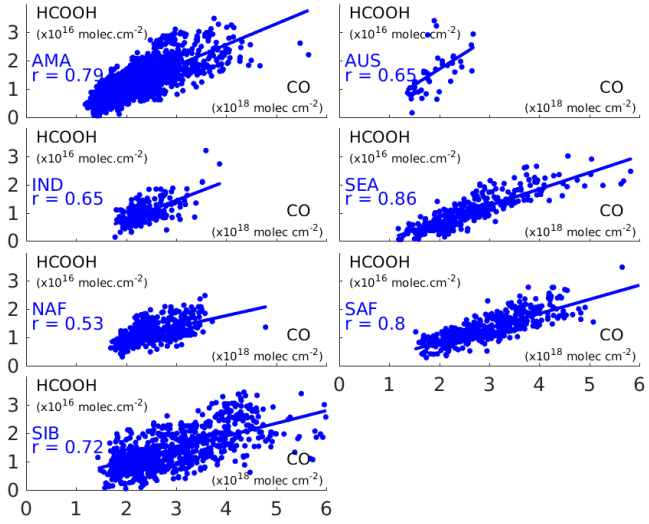

Figure 4. Scatterplots between the IASI fire-affected HCOOH total columns (in 10^{16} molec cm^{-2}) and the CO total columns (in 10^{18} molec cm^{-2}) over the seven regions (AMA = Amazonia, AUS = Australia, IND = India, SEA = Southeast Asia, NAF = northern Africa, SAF = southern Africa, SIB = Siberia). The linear regression is represented by the blue line and the correlation coefficient is also provided for each region.

5 Analysis of the data over the fire regions

5.1 Determination of the enhancement ratios

5.1.1 General analysis

Based on scatterplots in Fig. 4, an enhancement ratio can be calculated for each region. These enhancement ratios, defined as $ER_{(HCOOH/CO)}$, correspond to the value of the slope ∂[HCOOH] / ∂[CO] found in Fig. 4. This technique to determine the $ER_{(HCOOH/CO)}$ is more reliable than using only the columns themselves, i.e., by estimating an $ER_{(HCOOH/CO)}$ for each measurement pair (HCOOH, CO). Indeed, performing scatterplots helps to identify a common origin for HCOOH and CO. The values of the $ER_{(HCOOH/CO)}$ over each region are summarized in Table 2.

It is known that trace gas concentrations within smoke plumes can vary rapidly with time and are very sensitive to chemistry, so a comparison with previous work is always challenging, especially if these studies were performed over another altitude range, at a different location, or at a different period of the year.

A good agreement is, however, generally found with previous studies, even if it is important to keep in mind that an underestimation of our $ER_{(HCOOH/CO)}$ is possible due to the underestimation in the highest values of HCOOH as over the forest fires (see Sect. 2.3). On the other hand, the overestimation in the background column can also impact the calculation of our $ER_{(HCOOH/CO)}$. The effects of both biases are, however, limited since most of the HCOOH total columns used in our analysis over the selected regions are higher than 0.3×10^{16} molec cm^{-2} and lower than 2.5×10^{16} molec cm^{-2}, as explained in Sect. 2.3.

Nevertheless, in order to investigate the possible impact of the overestimation in the lower columns and the underestimation in the higher columns on the calculated ratios, a test was performed, by using only HCOOH columns with a thermal contrast (TC) larger than 10 K. Indeed, the increase in the thermal contrast (i.e., the temperature difference between the surface and the first layer in the retrieved profile) leads to reducing the detection limit as shown in Pommier al. (2016). This enhancement of the detection level helps to minimize the bias in the retrieved total columns as explained in Crevoisier et al. (2014). For the analysis performed here, similar slopes and correlation coefficients were generally calculated, suggesting a negligible effect of this parameter on the biases. The only exception is an increase in $ER_{(HCOOH/CO)}$ over Siberia ($6.5 \times 10^{-3} \pm 0.19 \times 10^{-3}$ mol mol^{-1} when using only IASI measurements with TC above 10 K against 4.4×10^{-3} mol mol$^{-1} \pm 0.09 \times 10^{-3}$ in Table 2). It is worth noting that only 48 % of the selected scenes remain over Siberia when applying this filter on thermal contrast (60 % for SEA, 77 % for AMA, 80 % for SAF, 83 % for AUS and NAF, and 89 % for IND). This implies that the statistics on the fire emissions in the higher latitudes of Siberia are dominated by measurements with a low thermal contrast and thus with HCOOH total columns with higher uncertainties. However, the limited changes in slopes and correlation coefficients give us confidence that the results presented in Table 2 are representative.

Table 2. Enhancement ratio of HCOOH relative to CO ($\mathrm{mol\,mol^{-1}}$) with its standard deviation compared to enhancement ratios of HCOOH relative to CO and emissions ratios of HCOOH reported in the literature for the seven studied regions.

Region	Enhancement ratio to CO ($\mathrm{mol\,mol^{-1}}$), this work	Enhancement ratio to CO ($\mathrm{mol\,mol^{-1}}$) found in literature	Emission ratio to CO ($\mathrm{mol\,mol^{-1}}$) found in literature	Instrument used
AMA	$7.3 \times 10^{-3} \pm 0.08 \times 10^{-3}$	$5.1 \times 10^{-3} \pm 1.5 \times 10^{-3}$ (González Abad et al., 2009)*		ACE-FTS
		$6.7 \times 10^{-3} \pm 2.1 \times 10^{-3}$ (Chaliyakunnel et al., 2016)		TES
AUS	$11.1 \times 10^{-3} \pm 1.37 \times 10^{-3}$	$4.5 \times 10^{-3} \pm 5.1 \times 10^{-3}$ (Chaliyakunnel et al., 2016)		TES
		$21.0 \times 10^{-3} \pm 10.0 \times 10^{-3}$ (Paton-Walsh et al., 2005)*		ground-based FTIR
IND	$6.8 \times 10^{-3} \pm 0.44 \times 10^{-3}$	None		–
SEA	$5.8 \times 10^{-3} \pm 0.15 \times 10^{-3}$	None		–
NAF	$4.0 \times 10^{-3} \pm 0.19 \times 10^{-3}$	$2.8 \times 10^{-3} \pm 0.4 \times 10^{-3}$ (Chaliyakunnel et al., 2016)		TES
SAF	$5.0 \times 10^{-3} \pm 0.13 \times 10^{-3}$	$2.6 \times 10^{-3} \pm 0.3 \times 10^{-3}$ (Chaliyakunnel et al., 2016)		TES
		$4.6 \times 10^{-3} \pm 0.3 \times 10^{-3}$ (Vigouroux et al., 2012)		ground-based FTIR
		5.1×10^{-3} (Coheur et al., 2007)		ACE-FTS
		$11.3 \times 10^{-3} \pm 7.6 \times 10^{-3}$ (Rinsland et al., 2006)*		ACE-FTS
			$5.9 \times 10^{-3} \pm 2.2 \times 10^{-3}$ (Yokelson et al., 2003)	airborne FTIR
			$5.1–8.7 \times 10^{-3}$ (Sinha al., 2003)	airborne FTIR
SIB	$4.4 \times 10^{-3} \pm 0.09 \times 10^{-3}$	$0.77–6.41 \times 10^{-3}$ (Tereszchuk et al., 2013)		ACE-FTS
		$2.69–15.93 \times 10^{-3}$ (Viatte et al., 2015)		ground-based FTIR
		$10.0–32.0 \times 10^{-3}$ (R'Honi et al., 2013)		IASI

* Their "emission ratios" are re-qualified as enhancement ratios in this study since their ratios were not measured at the origin the fire emission but at high altitudes and/or further downwind of the fires.

5.1.2 Analysis over each region

A few backward trajectories (along 5 days, not shown) have been calculated for our hotspots with the online version of the HYSPLIT atmospheric transport and dispersion modeling system (Rolph, 2017). These trajectories, initialized at different altitudes, confirm a main origin close to the surface of our IASI fire-affected columns. However, it is impossible to properly compare the origin of the air masses with previous studies as our studied period (2008–2014) or our studied fires do not necessarily match with plumes described in other publications. It is also difficult to estimate the age of our studied air masses by gathering the plumes during a 7-year period and without an accurate knowledge of the altitude of the plumes.

When compared with other studies, the best agreement for the values presented in Table 2 is found over southern Africa where the $\mathrm{ER_{(HCOOH/CO)}}$ ($5 \times 10^{-3} \pm 0.13 \times 10^{-3}\,\mathrm{mol\,mol^{-1}}$) is similar to the value calculated by Vigouroux et al. (2012) and Coheur et al. (2007). It also agrees with the broad range of values of emission ratios ($\mathrm{EmR_{(HCOOH/CO)}}$) referenced by Sinha et al. (2003). This result corroborates the relevance of the

methodology used in this work over this region for the identification of fire-affected IASI columns close to the source. Vigouroux et al. (2012) sampled biomass burning outflow of southern Africa and Coheur et al. (2007) calculated their $ER_{(HCOOH/CO)}$ in plumes observed over Tanzania in the upper troposphere, while Sinha et al. (2003) did it within plumes over Zambia at the origin of the fire.

A few assumptions are needed in order to interpret our $ER_{(HCOOH/CO)}$, but the analysis given hereafter is only indicative since these previous studies did not measure the same plumes as those presented in this work. Our $ER_{(HCOOH/CO)}$ is also calculated without making any distinction on the seasonal variation or on the type of biomass burning plumes sampled (e.g., emitted by a savanna fire or by a forest fire). The analysis by biome is presented in Sect. 5.2. Since these $ER_{(HCOOH/CO)}$ values from previous studies and the $EmR_{(HCOOH/CO)}$ from Sinha et al. (2003) agree with our $ER_{(HCOOH/CO)}$, and since HCOOH has a short lifetime, this may suggest that the selected plumes measured by IASI from 2008 to 2014 and those sampled by Vigouroux et al. (2012) and Coheur et al. (2007) encountered a limited secondary production or a low sink (deposition or reaction with OH in the troposphere during their transport). To quantify the role of the chemistry or of the deposition within the plumes, a modeling work should be performed. However, this is beyond the scope of this paper.

Another important point is that the decay of HCOOH is faster than that of CO. As our $ER_{(HCOOH/CO)}$ is similar to the $ER_{(HCOOH/CO)}$ from the other studies and to the $EmR_{(HCOOH/CO)}$ given in Sinha et al. (2003), this could suggest that all these plumes (from our study, from Vigouroux et al., 2012, and from Coheur et al., 2007) are rapidly advected in the troposphere. Our $ER_{(HCOOH/CO)}$ differs from the value in Rinsland et al. (2006) ($11.3 \times 10^{-3} \pm 7.6 \times 10^{-3}$ mol mol^{-1}), since our ratio is 55 % lower. One possible explanation is the multi-origin of the plumes studied by Rinsland et al. (2006), since, based on their backward trajectories, their plumes could be influenced by biomass burning originating from southern Africa and/or from South America. The travel during the few days across the Atlantic Ocean may explain the change in their $ER_{(HCOOH/CO)}$.

It is worth noting that the ACE-FTS instrument used in their study works in a limb solar occultation mode. This means that the atmospheric density sampled by the instrument is larger than the one measured by the nadir geometry with IASI. However, the difference in geometry cannot explain why we find an agreement with the ACE-FTS measurement values reported by Coheur et al. (2007) and a disagreement with those from Rinsland et al. (2006). Part of the difference could be associated with the difference in the assumptions used in both retrievals (e.g., the a priori profile).

The $ER_{(HCOOH/CO)}$ from our work is also 15 % lower than the $EmR_{(HCOOH/CO)}$ in Yokelson et al. (2003) ($5.9 \times 10^{-3} \pm 2.2 \times 10^{-3}$ mol mol^{-1}), who calculated their value within plumes over Zambia, Zimbabwe, and South Africa. With this difference we can also suggest the presence of a sink of HCOOH within the plumes detected by IASI or that this slight underestimation is simply related to the faster decay of HCOOH than that of CO. Conversely, the $ER_{(HCOOH/CO)}$ retrieved from IASI is twice that of Chaliyakunnel et al. (2016) ($2.6 \times 10^{-3} \pm 0.3 \times 10^{-3}$ mol mol^{-1}). Chaliyakunnel et al. (2016) developed an approach allowing the determination of pyrogenic $ER_{(HCOOH/CO)}$ by reducing the impact of the mix with the ambient air. To do so, they calculated the $ER_{(HCOOH/CO)}$ in the vicinity of the fire count from MODIS (averaged in a cell having the resolution of the GEOS-Chem model, i.e., $2° \times 2.5°$) and they differentiated this value with a background $ER_{(HCOOH/CO)}$ defined by the concentrations distant from these fires. They concluded that their most reliable value on the amount of HCOOH produced from fire emissions was obtained from African fires.

Over northern Africa, the calculated $ER_{(HCOOH/CO)}$ ($4 \times 10^{-3} \pm 0.19 \times 10^{-3}$ mol mol^{-1}) is 42 % higher than the $ER_{(HCOOH/CO)}$ calculated in Chaliyakunnel et al. (2016) ($2.8 \times 10^{-3} \pm 0.4 \times 10^{-3}$ mol mol^{-1}). It is worth noting that NAF is the region characterized by a scatterplot with the lowest correlation coefficient (Fig. 4).

A larger difference is found over Australia where the $ER_{(HCOOH/CO)}$ is $11.1 \times 10^{-3} \pm 1.37 \times 10^{-3}$ mol mol^{-1}. This $ER_{(HCOOH/CO)}$ is roughly the mean of both values reported by Paton-Walsh et al. (2005) and Chaliyakunnel et al. (2016). The difference between our work and that of Paton-Walsh et al. (2005) may be explained by the different origin of the probed plume. In our case, the studied area corresponds to the northern part of the Northern Territory with savanna-type vegetation (as shown in Sect. 5.2), while Paton-Walsh et al. (2005) sampled bush fire plumes coming from the eastern coast of Australia, representative of Australian temperate forest. In the work done by Chaliyakunnel et al. (2016), a quite uncertain value is reported ($4.5 \times 10^{-3} \pm 5.1 \times 10^{-3}$ mol mol^{-1}), with an error larger than their $ER_{(HCOOH/CO)}$.

Over Amazonia, our $ER_{(HCOOH/CO)}$ ($7.3 \times 10^{-3} \pm 0.08 \times 10^{-3}$ mol mol^{-1}) is similar to the value given in Chaliyakunnel et al. (2016), who report a larger bias over Amazonia. Over this region, our $ER_{(HCOOH/CO)}$ is higher than the one obtained by González Abad et al. (2009) with ACE-FTS in the upper troposphere ($5.1 \times 10^{-3} \pm 1.5 \times 10^{-3}$ mol mol^{-1}). This difference with the study done by González Abad et al. (2009) may be explained by the difference in the altitude of the detection of the forest fire plume between IASI (mid-troposphere) and ACE-FTS (upper troposphere) and thus by a difference in the ongoing chemistry within their respective sampled plumes. The geometry of the sampling (nadir vs. limb) or the difference in the retrieval may also have an impact in the retrieved HCOOH.

The Siberian $ER_{(HCOOH/CO)}$ (4.4×10^{-3} mol mol^{-1} $\pm 0.09 \times 10^{-3}$) is found to be in good agreement with the wide range of values obtained by Tereszchuk et al. (2013) and Viatte et al. (2015). This $ER_{(HCOOH/CO)}$ is, however, lower than the ratios calculated by R'Honi et al. (2013), who focused on the extreme fire event that occurred in 2010.

For India and Southeast Asia, a comparison is not possible since no previous studies were reported. The comparison is performed next, based on the emission factors.

5.2 Analysis based on the type of vegetation

We have complemented our comparison of the enhancement ratios by comparing our ratios to emissions ratios calculated from emission factors found in literature. The main argument for performing such comparison is the lack of measurements of enhancement ratios over IND and SEA. Furthermore, such comparison from emission factors facilitates an analysis based on hypotheses about the type of vegetation burned.

Even if our methodology attempts to characterize the HCOOH emitted by biomass burning close to the source, our columns are probably not representative of the emission at the origin of the fire. The altitude of the sampling (mid-troposphere), even if an influence from the surface is shown, and the age of the plumes (at least a few hours) have a large impact on our enhancement ratios.

To perform a proper comparison with emission ratios, our enhancement ratios should be converted to emission ratios. To do so, it would be essential to take into account the decay of the compounds during the transport of the plume. However, due to the methodology used, i.e., averaging the data collected during a few hours (between 0 and 5 h from the time registered by MODIS for each detected fire), the calculation of the decay of each compound is not possible. We therefore have compared our enhancement ratios to emission ratios, and the comparison presented hereafter is mostly illustrative.

For both IND and SEA regions, the emission ratios have been calculated from the emission factors provided in Akagi et al. (2011). For the other regions, in addition to the values from Akagi et al. (2011), emission ratios were similarly calculated from emission factors given in other studies (listed in Table 3).

Based on the emission ratios, the emission factors are usually derived by this following equation:

$$EF_{HCOOH} = EF_{CO} \times MW_{HCOOH}/MW_{CO} \times EmR_{(HCOOH/CO)}. \quad (1)$$

EF_{HCOOH} is the emission factor for HCOOH; $EmR_{(HCOOH/CO)}$ is the molar emission ratio of HCOOH with respect to CO; MW_{HCOOH} is the molecular weight of HCOOH; MW_{CO} is the molecular weight of CO; and EF_{CO} is the emission factor for CO for dry matter, set to the value taken from Akagi et al. (2011).

Thus, based on Eq. (1), $EmR_{(HCOOH/CO)}$ values were calculated and compared with our $ER_{(HCOOH/CO)}$ (Table 3). In this calculation, the vegetation type characterizing each region is important. Some regions are composed of a mix of vegetation types as shown in Fig. 1. This is, for example, the case for AMA and SAF (e.g., White, 1981). Thus, following the classification from Akagi et al. (2011), AMA and SAF are composed of tropical forest and savanna, characterized by an EF_{CO} of 93 ± 27 and 63 ± 17 g kg^{-1}, respectively (Akagi et al., 2011). AUS and NAF correspond to a savanna fuel type. SIB is a boreal forest area with an EF_{CO} of 127 ± 45 g kg^{-1}. Based also on the maps shown by Fig. 9 in Schreier et al. (2014) and Fig. 13 in van der Werf et al. (2010), the soil for IND is supposed to be mainly composed of cropland (agriculture), which is associated with an EF_{CO} of 102 ± 33 g kg^{-1}, and probably also by extratropical forest, which is characterized by an EF_{CO} equal to 122 ± 44 g kg^{-1}, and savanna, with an EF_{CO} of 63 ± 17 g kg^{-1}. The fuel type for SEA is supposed to be a mix of extratropical forest and savanna, with an EF_{CO} of 122 ± 44 and 63 ± 17 g kg^{-1}, respectively. Cropland fuel type was also used, since large agricultural biomass burning is occurring in this region (e.g., Duc et al., 2016).

In addition to the $EmR_{(HCOOH/CO)}$ calculated from the EF_{HCOOH} given in the literature, a classification for our $ER_{(HCOOH/CO)}$ has also been done, based on the data from the MCD12Q1 product. As each hotspot is associated with a land cover value defined by the MCD12Q1 product, enhancement ratios by biome have been calculated. The limitations of this dataset are its coarse resolution ($0.5° \times 0.5°$) and the lack of seasonal variation. It gives supplementary information on the type of fuel burned identified by MODIS. The corresponding $ER_{(HCOOH/CO)}$ values are provided in Table 3. Only the values calculated from a scatterplot with a correlation coefficient higher than 0.4 are reported.

Despite the assumptions made, a fair agreement is found over southern Africa. Our $ER_{(HCOOH/CO)}$ ($5 \times 10^{-3} \pm 0.13 \times 10^{-3}$ mol mol^{-1}) is indeed similar to the $EmR_{(HCOOH/CO)}$ calculated from Sinha et al. (2004) by using savanna fuel type, and the $ER_{(HCOOH/CO)}$ is between both values calculated from Yokelson et al. (2003). This agreement is consistent since both previous studies sampled plumes emitted by savanna fires. Yokelson et al. (2003) and Sinha et al. (2004) both used the same sampling strategy. They sampled fire plumes by penetrating several minutes-old plumes at relatively low altitude (up to 1.3 km for Sinha et al., 2004, and just above the flame front for Yokelson et al., 2003). This agreement shows, as already described in the previous section, that our $ER_{(HCOOH/CO)}$ over southern Africa is similar to their $EmR_{(HCOOH/CO)}$. It is also noteworthy, based on the MODIS land-cover-type product, that all the studied hotspots are defined as savanna fires. On other hand, our $ER_{(HCOOH/CO)}$ is also similar to the

Table 3. Enhancement ratio of HCOOH relative to CO (mol mol^{-1}) with its standard deviation and enhancement ratio of HCOOH relative to CO (mol mol^{-1}) by biome with its standard deviation calculated in this work. For each enhancement ratio by biome, the correlation coefficient and the number of MODIS hotspots are provided. The enhancement ratios are compared to emission ratios calculated from emission factors given in the literature for the seven studied regions. For the calculation of these emission ratios, the emission factors of CO for the corresponding fuel type given in Akagi et al. (2011) are used. Emission ratios of HCOOH relative to CO (mol mol^{-1}) calculated from the emission factors of HCOOH given in Akagi et al. (2011) for the corresponding fuel type are also provided.

Region	Enhancement ratio to CO (mol mol^{-1}), this work	Enhancement ratio to CO (mol mol^{-1})[a] by biome[b], this work	Emission ratio to CO (mol mol^{-1}) calculated from EF_{HCOOH} given in literature and using EF_{CO} from Akagi et al. (2011)	Instrument used
AMA	$7.3 \times 10^{-3} \pm 0.08 \times 10^{-3}$	$6.3 \times 10^{-3} \pm 0.22 \times 10^{-3}$ (evergreen broadleaf forest, $r = 0.81$, $n = 454$) $3.0 \times 10^{-3} \pm 0.81 \times 10^{-3}$ (open shrubland, $r = 0.91$, $n = 5$) $7.0 \times 10^{-3} \pm 2.47 \times 10^{-3}$ (woody savanna, $r = 0.63$, $n = 14$) $7.6 \times 10^{-3} \pm 0.09 \times 10^{-3}$ (savanna, $r = 0.79$, $n = 3909$) $8.4 \times 10^{-3} \pm 0.39 \times 10^{-3}$ (grassland, $r = 0.88$, $n = 143$) $4.6 \times 10^{-3} \pm 0.35 \times 10^{-3}$ (cropland, $r = 0.88$, $n = 54$)	1.8×10^{-3} – tropical forest (Yokelson et al., 2007, 2008)[c] 2.7×10^{-3} – savanna (Yokelson et al., 2007, 2008)[c] 2.0×10^{-3} – savanna (Akagi et al., 2011) 5.2×10^{-3} – tropical forest (Akagi et al., 2011)	airborne FTIR (Yokelson et al., 2007); laboratory (Yokelson et al., 2008); catalog
AUS	$11.1 \times 10^{-3} \pm 1.37 \times 10^{-3}$	$5.7 \times 10^{-3} \pm 2.55 \times 10^{-3}$ (woody savanna, $r = 0.6$, $n = 11$) $11.2 \times 10^{-3} \pm 1.49 \times 10^{-3}$ (savanna, $r = 0.65$, $n = 80$)	2.0×10^{-3} – savanna (Akagi et al., 2011)	catalog
IND	$6.8 \times 10^{-3} \pm 0.44 \times 10^{-3}$	$6.6 \times 10^{-3} \pm 0.77 \times 10^{-3}$ (woody savanna, $r = 0.65$, $n = 103$) $6.2 \times 10^{-3} \pm 0.62 \times 10^{-3}$ (cropland, $r = 0.58$, $n = 198$) $8.8 \times 10^{-3} \pm 1.19 \times 10^{-3}$ (cropland/natural vegetation mosaic, $r = 0.85$, $n = 23$)	2.0×10^{-3} – savanna (Akagi et al., 2011) 2.7×10^{-3} – extratropical forest (Akagi et al., 2011) 6.0×10^{-3} – cropland (Akagi et al., 2011)	catalog
SEA	$5.8 \times 10^{-3} \pm 0.15 \times 10^{-3}$	$5.6 \times 10^{-3} \pm 0.20 \times 10^{-3}$ (evergreen broadleaf forest, $r = 0.83$, $n = 334$) $6.3 \times 10^{-3} \pm 0.66 \times 10^{-3}$ (mixed forest, $r = 0.76$, $n = 70$) $6.2 \times 10^{-3} \pm 0.38 \times 10^{-3}$ (woody savanna, $r = 0.86$, $n = 99$) $7.1 \times 10^{-3} \pm 0.99 \times 10^{-3}$ (cropland/natural vegetation mosaic, $r = 0.84$, $n = 23$)	2.0×10^{-3} – savanna (Akagi et al., 2011) 2.7×10^{-3} – extratropical forest (Akagi et al., 2011) 6.0×10^{-3} – cropland (Akagi et al., 2011)	catalog
NAF	$4.0 \times 10^{-3} \pm 0.19 \times 10^{-3}$	$3.4 \times 10^{-3} \pm 0.63 \times 10^{-3}$ (evergreen broadleaf forest, $r = 0.52$, $n = 78$) $3.3 \times 10^{-3} \pm 0.28 \times 10^{-3}$ (woody savanna, $r = 0.44$, $n = 569$) $4.4 \times 10^{-3} \pm 0.29 \times 10^{-3}$ (savanna, $r = 0.59$, $n = 441$) $22.6 \times 10^{-3} \pm 11.06 \times 10^{-3}$ (cropland/natural vegetation mosaic, $r = 0.67$, $n = 7$)	2.0×10^{-3} – savanna (Akagi et al., 2011)	catalog

Table 3. Continued.

Region	Enhancement ratio to CO (mol mol^{-1}), this work	Enhancement ratio to CO (mol mol^{-1})[a] by biome[b], this work	Emission ratio to CO (mol mol^{-1}) calculated from EF_{HCOOH} given in literature and using EF_{CO} from Akagi et al. (2011)	Instrument used
SAF	$5.0 \times 10^{-3} \pm 0.13 \times 10^{-3}$	all hotspots are woody savanna	3.3×10^{-3} – tropical forest (Sinha et al., 2004)[d] 4.8×10^{-3} – savanna (Sinha et al., 2004)[d]	airborne FTIR
			4.1×10^{-3} – tropical forest (Yokelson et al., 2003) 6.0×10^{-3} – savanna (Yokelson et al., 2003)	airborne FTIR
			13×10^{-3} – tropical forest (Rinsland et al., 2006) 19.2×10^{-3} – savanna (Rinsland et al., 2006)	ACE-FTS
			2.0×10^{-3} – savanna (Akagi et al., 2011) 5.2×10^{-3} – tropical forest (Akagi et al., 2011)	catalog
SIB	$4.4 \times 10^{-3} \pm 0.09 \times 10^{-3}$	$4.0 \times 10^{-3} \pm 0.31 \times 10^{-3}$ (evergreen needleleaf forest, $r = 0.63$, $n = 245$) $3.6 \times 10^{-3} \pm 0.16 \times 10^{-3}$ (deciduous needleleaf forest, $r = 0.66$, $n = 659$) $3.4 \times 10^{-3} \pm 0.18 \times 10^{-3}$ (mixed forest, $r = 0.57$, $n = 759$) $6.6 \times 10^{-3} \pm 0.48 \times 10^{-3}$ (open shrubland, $r = 0.76$, $n = 143$) $6.0 \times 10^{-3} \pm 0.41 \times 10^{-3}$ (woody savanna, $r = 0.76$, $n = 155$) $3.8 \times 10^{-3} \pm 0.65 \times 10^{-3}$ (permanent wetland, $r = 0.6$, $n = 63$)	2.7×10^{-3} – boreal forest (Akagi et al., 2011)	catalog

[a] Only the enhancement ratios to CO calculated from a scatterplot with a correlation coefficient higher than 0.4 are reported. [b] The type of vegetation is defined by the land-cover-type data product (MCD12Q1). [c] The EF_{HCOOH} values were corrected based on the comment from Yokelson et al. (2013) (EF_{HCOOH} used: 0.281 for Yokelson et al., 2007; 0.2767 for Yokelson et al., 2008). [d] The means of both EF_{HCOOH} values provided in Sinha et al. (2004) were used for our $EmR_{HCOOH/CO}$ calculation.

$EmR_{(HCOOH/CO)}$ from Akagi et al. (2011) but for the tropical forest. A large underestimation compared to Rinsland et al. (2006) is found. This underestimation confirms the disagreement with their study already shown in Table 2.

Over northern Africa, our $ER_{(HCOOH/CO)}$ is twice as large as the $EmR_{(HCOOH/CO)}$ provided by Akagi et al. (2011), probably due to the lower correlation found in our scatterplot. It is highly probable that our presumed fire-affected IASI columns are indeed impacted by other air masses. The land classification based on the MODIS product also shows a diverse origin of the hotspots.

For Amazonia, the calculated $ER_{(HCOOH/CO)}$ ($7.3 \times 10^{-3} \pm 0.08 \times 10^{-3}$ mol mol^{-1}) is close to the $EmR_{(HCOOH/CO)}$ given in Akagi et al. (2011) for the tropical forest (5.2×10^{-3} mol mol^{-1}), but it is 3 times higher than the values derived from Yokelson et al. (2007, 2008) for the same vegetation type. For the latter, it is worth noting that their factors have been corrected a posteriori (scaled down by a factor of 2.1), as described in their comment following the paper done by R'Honi et al. (2013) (see Yokelson et al., 2013). As Yokelson et al. (2007, 2008) sampled the forest fire plumes by penetrating recent columns of smoke 200–1000 m above the flame front, our $ER_{(HCOOH/CO)}$ may reflect a secondary production of HCOOH. This assumed secondary production is less substantial if we compare with the $EmR_{(HCOOH/CO)}$ from Akagi et al. (2011). The classification based on the type of fuel burned shows a diverse origin of the fire plumes over Amazonia. Six biomes

have been identified following the classification from the MCD12Q1 product.

Over Australia and over Siberia, the calculated $ER_{(HCOOH/CO)}$ is overestimated compared to the $EmR_{(HCOOH/CO)}$ given in Akagi et al. (2011) for a savanna fire and for a boreal forest, respectively. If our value for near-source estimation is correct, this would probably mean that the direct emission is underestimated (by 450 % over Australia and by 60 % over Siberia) or that a large secondary production of HCOOH from Australian and Siberian fires occurred. These hypotheses in biased emissions and/or secondary production need to be verified with modeling studies. Over Australia, the difference is very large even though the comparison done by Pommier al. (2016) with FTIR measurements showed that the lowest bias was found for the Australian site (−2 % at Wollongong). Over Siberia, we also note that the region is characterized by fires emitted from six types of biome based on the classification from MODIS.

Finally, in this comparison, the studied plumes over India and Southeast Asia are certainly related to agricultural fires, even if the evergreen broadleaf forest seems to dominate in the MODIS land-cover-type product. This is strongly possible as agricultural residue burning is prevalent in these regions (e.g., Kaskaoutis et al., 2014; Vadrevu et al., 2015). Over India and over Southeast Asia, our $ER_{(HCOOH/CO)}$ values ($6.8 \times 10^{-3} \pm 0.44 \times 10^{-3}$ mol mol^{-1} for India and $5.8 \times 10^{-3} \pm 0.15 \times 10^{-3}$ mol mol^{-1} for Southeast Asia) are close to the value referenced by Akagi et al. (2011) for cropland fires (6×10^{-3} mol mol^{-1}). Since our $ER_{(HCOOH/CO)}$ values are close to the $EmR_{(HCOOH/CO)}$ derived from the EF_{HCOOH} in Akagi et al. (2011), this may suggests that the plumes studied over the 7-year period correspond to fresh plumes where the chemistry or the physical sink is small. This is further supported by the fact that among the seven regions, IND and SEA have larger vertical velocity means close to the surface, indicating a larger rising motion of the air masses (not shown).

In general, the $ER_{(HCOOH/CO)}$ calculated for a specific biome varies with the regions. This shows that the type of vegetation is not the only factor influencing the $ER_{(HCOOH/CO)}$. The ongoing chemistry within a plume is important, and the age of the air masses impact the level of HCOOH and CO in the plumes.

6 Conclusions

A total of 7 years of HCOOH data measured by IASI over seven different fire regions around the world were analyzed (AMA, Amazonia; AUS, Australia; IND, India; SEA, Southeast Asia; NAF, northern Africa; SAF, southern Africa; SIB, Siberia). By taking into account the surface wind speed and by characterizing each MODIS fire hotspot with a value of HCOOH and CO total columns, this work established enhancement ratios for the seven biomass burning areas and compared them to previously reported values found in literature.

The difficulties in performing such a comparison are associated with the difference in locations, altitude of the sampling, and age of each fire plume studied in these previous publications. However, a fair agreement was found for the enhancement ratios calculated in this work, in comparison with other studies, using satellite, airborne, or FTIR measurements.

In agreement with previous studies, the plumes from southern African savanna fires may reflect a limited secondary production or a limited sink occurring in the upper layers of the troposphere during their transport. Such assumptions, however, are difficult to verify by comparing individual plumes (from previous studies) with plumes gathered during a 7-year period (from IASI) and remain speculative without a detailed modeling study. Plumes from agricultural fires over India and Southeast Asia probably correspond to fresh plumes as our $ER_{(HCOOH/CO)}$ values based on the 7-year IASI measurements are similar to the $EmR_{(HCOOH/CO)}$ values calculated from emission factors provided by Akagi et al. (2011).

A very good agreement in $ER_{(HCOOH/CO)}$ was found over Amazonia, especially in comparison with the work done by Chaliyakunnel et al. (2016), who determined pyrogenic $ER_{(HCOOH/CO)}$.

Fires over Australia and over Siberia are probably underestimated in terms of direct emission or secondary production of HCOOH. The analysis over Australia is, however, complicated as our $ER_{(HCOOH/CO)}$ approximately corresponds to the mean of the values reported in Paton-Walsh et al. (2005) and in Chaliyakunnel et al. (2016), and it is also 450 % higher than the $EmR_{(HCOOH/CO)}$ derived from Akagi et al. (2011). The underestimation by 60 % over Siberia is consistent with conclusions given in R'Honi et al. (2013). The calculation of the $ER_{(HCOOH/CO)}$ by biome shows that Siberian plumes are related to the burning of six different vegetation classes. The underestimation reported is thus difficult to confirm without the use of a chemical transport model.

The values found over northern Africa were more difficult to interpret as this region is characterized by a poorer correlation between our fire-affected HCOOH and CO total columns.

Finally, the estimation of the $ER_{(HCOOH/CO)}$ calculated by the type of vegetation burned, as referenced in the MODIS product, varies with the regions. This shows that other parameters than the type of fuel burned also influence the $ER_{(HCOOH/CO)}$.

With these findings and by updating the enhancement ratios, an interesting modeling study could be performed to estimate a new tropospheric budget for HCOOH. This IASI dataset may also be used in the future to study a single plume at different times to inform on the loss during transport. Further insight into the transport and chemistry may be gained

by using IASI's capability to measure several fire species simultaneously, such as HCN or C_2H_2 (e.g., Duflot et al., 2015). This would be useful for the characterization of the chemistry ongoing in a fire plume outflow.

An intercomparison with other space-borne instruments such as TES and ACE-FTS will be helpful to interpret the difference and the biases between the retrieved HCOOH columns and thus between their respective $ER_{(HCOOH/CO)}$ values.

Data availability. The IASI FORLI-CO and HCOOH products are publicly available via the Aeris data infrastructure, using the following links: http://iasi.aeris-data.fr/CO/ and http://iasi.aeris-data.fr/HCOOH/.

Competing interests. The authors declare that they have no conflict of interest.

Acknowledgements. The IASI mission is a joint mission of EUMETSAT and the Centre National d'Etudes Spatiales (CNES, France). The IASI L1 data are distributed in near real time by EUMETSAT through the EUMETCast system distribution. We thank the MODIS team for providing public access to fire products MCD14ML and the land-cover-type data product MCD12Q1. This MCD14ML MODIS dataset was provided by the University of Maryland and NASA FIRMS operated by NASA/GSFC/ESDIS with funding provided by NASA/HQ. The authors thank Simon Whitburn (ULB) for his help on the MODIS files. They also thank Juliette Hadji-Lazaro (LATMOS) and Lieven Clarisse (ULB) for preparing the IASI ΔT_b dataset. The authors also acknowledge ECMWF for free access to the meteorological data.

Edited by: Paul Monks
Reviewed by: two anonymous referees

References

Akagi, S. K., Yokelson, R. J., Wiedinmyer, C., Alvarado, M. J., Reid, J. S., Karl, T., Crounse, J. D., and Wennberg, P. O.: Emission factors for open and domestic biomass burning for use in atmospheric models, Atmos. Chem. Phys., 11, 4039–4072, https://doi.org/10.5194/acp-11-4039-2011, 2011.

Andreae, M. O., Andreae, T. W., Talbot, R. W., and Harriss, R. C.: Formic and acetic acid over the central Amazon region, Brazil, I. Dry season, J. Geophys. Res., 93, 1616–1624, https://doi.org/10.1029/JD093iD02p01616, 1988.

Andrews, D. U., Heazlewood, B. R., Maccarone, A. T., Conroy, T., Payne, R. J., Jordan, M. J. T., and Kable, S. H.: Photo-tautomerization of acetaldehyde to vinyl alcohol: a potential route to tropospheric acids, Science, 337, 1203–1206, https://doi.org/10.1126/science.1220712, 2012.

Beirle, S., Boersma, K. F., Platt, U., Lawrence, M. G., and Wagner, T.: Megacity emissions and lifetimes of nitrogen oxides probed from space, Science, 333, 1737–1739, https://doi.org/10.1126/science.1207824, 2011.

Bisht, D. S., Tiwari, S., Srivastava, A. K., Singh, J. V., Singh, B. P., and Srivastava, M. K.: High concentration of acidic species in rainwater at Varanasi in the Indo-Gangetic Plains, India, Nat. Hazards, 75, 2985–3003, https://doi.org/10.1007/s11069-014-1473-0, 2014.

Bohn, B., Siese, M., and Zetzschn, C.: Kinetics of the $OH + C_2H_2$ reaction in the presence of O_2, J. Chem. Soc. Faraday T., 92, 1459–1466, 1996.

Cady-Pereira, K. E., Chaliyakunnel, S., Shephard, M. W., Millet, D. B., Luo, M., and Wells, K. C.: HCOOH measurements from space: TES retrieval algorithm and observed global distribution, Atmos. Meas. Tech., 7, 2297–2311, https://doi.org/10.5194/amt-7-2297-2014, 2014.

Chaliyakunnel, S., Millet, D. B., Wells, K. C., Cady-Pereira, K. E., and Shephard, M. W.: A Large Underestimate of Formic Acid from Tropical Fires: Constraints from Space-Borne Measurements, Environ. Sci. Technol., 50, 5631–5640, https://doi.org/10.1021/acs.est.5b06385, 2016.

Chameides, W. L. and Davis, D. D.: Aqueous-phase source of formic acid in clouds, Nature, 304, 427–429, 1983.

Channan, S., Collins, K., and Emanuel, W. R.: Global mosaics of the standard MODIS land cover type data. University of Maryland and the Pacific Northwest National Laboratory, College Park, Maryland, USA, 2014.

Clerbaux, C., Boynard, A., Clarisse, L., George, M., Hadji-Lazaro, J., Herbin, H., Hurtmans, D., Pommier, M., Razavi, A., Turquety, S., Wespes, C., and Coheur, P.-F.: Monitoring of atmospheric composition using the thermal infrared IASI/MetOp sounder, Atmos. Chem. Phys., 9, 6041–6054, https://doi.org/10.5194/acp-9-6041-2009, 2009.

Clubb, A. E., Jordan, M. J. T., Kable, S. H., and Osborn, D. L.: Phototautomerization of Acetaldehyde to vinyl alcohol: a primary process in UV-irradiated acetaldehyde from 295 to 335 nm, J. Phys. Chem. Lett., 3, 3522–3526, 2012.

Coheur, P.-F., Herbin, H., Clerbaux, C., Hurtmans, D., Wespes, C., Carleer, M., Turquety, S., Rinsland, C. P., Remedios, J., Hauglustaine, D., Boone, C. D., and Bernath, P. F.: ACE-FTS observation of a young biomass burning plume: first reported measurements of C_2H_4, C_3H_6O, H_2CO and PAN by infrared occultation from space, Atmos. Chem. Phys., 7, 5437–5446, https://doi.org/10.5194/acp-7-5437-2007, 2007.

Coheur, P.-F., Clarisse, L., Turquety, S., Hurtmans, D., and Clerbaux, C.: IASI measurements of reactive trace species in biomass burning plumes, Atmos. Chem. Phys., 9, 5655–5667, https://doi.org/10.5194/acp-9-5655-2009, 2009.

Crevoisier, C., Chédin, A., Matsueda, H., Machida, T., Armante, R., and Scott, N. A.: First year of upper tropospheric integrated content of CO_2 from IASI hyperspectral infrared observations, Atmos. Chem. Phys., 9, 4797–4810, https://doi.org/10.5194/acp-9-4797-2009, 2009.

Crevoisier, C., Clerbaux, C., Guidard, V., Phulpin, T., Armante, R., Barret, B., Camy-Peyret, C., Chaboureau, J.-P., Coheur, P.-F., Crépeau, L., Dufour, G., Labonnote, L., Lavanant, L., Hadji-Lazaro, J., Herbin, H., Jacquinet-Husson, N., Payan, S., Péquignot, E., Pierangelo, C., Sellitto, P., and Stubenrauch, C.: Towards IASI-New Generation (IASI-NG): impact of improved spectral resolution and radiometric noise on the retrieval of thermody-

namic, chemistry and climate variables, Atmos. Meas. Tech., 7, 4367–4385, https://doi.org/10.5194/amt-7-4367-2014, 2014.

Dee, D. P., Uppala, S. M., Simmons, A. J., Berrisford, P., Poli, P., Kobayashi, S., Andrae, U., Balmaseda, M. A., Balsamo, G., Bauer, P., Bechtold, P., Beljaars, A. C. M., van de Berg, L., Bidlot, J., Bormann, N., Delsol, C., Dragani, R., Fuentes, M., Geer, A. J., Haimberger, L., Healy, S. B., Hersbach, H., Hólm, E. V., Isaksen, L., Kållberg, P., Köhler, M., Matricardi, M. , McNally, A. P., Monge-Sanz, B. M., Morcrette, J.-J., Park, B.-K., Peubey, C., de Rosnay, P., Tavolato, C., Thépaut, J.-N., and Vitart, F.: The ERA-Interim reanalysis: configuration and performance of the data assimilation system, Q. J. Roy. Meteor. Soc., 137, 553–597, https://doi.org/10.1002/qj.828, 2011.

Duflot, V., Wespes, C., Clarisse, L., Hurtmans, D., Ngadi, Y., Jones, N., Paton-Walsh, C., Hadji-Lazaro, J., Vigouroux, C., De Mazière, M., Metzger, J.-M., Mahieu, E., Servais, C., Hase, F., Schneider, M., Clerbaux, C., and Coheur, P.-F.: Acetylene (C_2H_2) and hydrogen cyanide (HCN) from IASI satellite observations: global distributions, validation, and comparison with model, Atmos. Chem. Phys., 15, 10509–10527, https://doi.org/10.5194/acp-15-10509-2015, 2015.

De Wachter, E., Barret, B., Le Flochmoën, E., Pavelin, E., Matricardi, M., Clerbaux, C., Hadji-Lazaro, J., George, M., Hurtmans, D., Coheur, P.-F., Nedelec, P., and Cammas, J. P.: Retrieval of MetOp-A/IASI CO profiles and validation with MOZAIC data, Atmos. Meas. Tech., 5, 2843–2857, https://doi.org/10.5194/amt-5-2843-2012, 2012.

Duc, H. N., Bang, H. Q., and Quang, N. X.: Modelling and prediction of air pollutant transport during the 2014 biomass burning and forest fires in peninsular Southeast Asia, Environ. Monit. Assess, 188, 106, https://doi.org/10.1007/s10661-016-5106-9, 2016.

Fioletov, V. E., McLinden, C. A., Krotkov, N., and Li, C.: Lifetimes and emissions of SO_2 from point sources estimated from OMI, Geophys. Res. Lett., 42, 1969–1976, https://doi.org/10.1002/2015GL063148, 2015.

Friedl, M. A., Sulla-Menashe, D., Tan, B., Schneider, A., Ramankutty, N., Sibley, A., and Huang, X., MODIS Collection 5 global land cover: Algorithm refinements and characterization of new datasets, 2001–2012, Collection 5.1 IGBP Land Cover, Remote Sens. Environ., 114, 168–182, https://doi.org/10.1016/j.rse.2009.08.016, 2010.

Gabriel, R., Schäfer, L., Gerlach, C., Rausch, T., and Kesselmeier, J.: Factors controlling the emissions of volatile organic acids from leaves of *Quercus ilex* L. (Holm oak), Atmos. Environ., 33, 1347–1355, 1999.

George, M., Clerbaux, C., Hurtmans, D., Turquety, S., Coheur, P.-F., Pommier, M., Hadji-Lazaro, J., Edwards, D. P., Worden, H., Luo, M., Rinsland, C., and McMillan, W.: Carbon monoxide distributions from the IASI/METOP mission: evaluation with other space-borne remote sensors, Atmos. Chem. Phys., 9, 8317–8330, https://doi.org/10.5194/acp-9-8317-2009, 2009.

Giglio, L.: MODIS Collection 5 Active Fire Product User's Guide, v2.5, available at: http://modis-fire.umd.edu/pages/manuals.php or http://modis-fire.umd.edu/files/MODIS_Fire_Users_Guide_2.5.pdf (last access: 31 March 2013), 2013.

Giglio, L., van der Werf, G. R., Randerson, J. T., Collatz, G. J., and Kasibhatla, P.: Global estimation of burned area using MODIS active fire observations, Atmos. Chem. Phys., 6, 957–974, https://doi.org/10.5194/acp-6-957-2006, 2006.

González Abad, G., Bernath, P. F., Boone, C. D., McLeod, S. D., Manney, G. L., and Toon, G. C.: Global distribution of upper tropospheric formic acid from the ACE-FTS, Atmos. Chem. Phys., 9, 8039–8047, https://doi.org/10.5194/acp-9-8039-2009, 2009.

Goode, J., Yokelson, R., Ward, D., Susott, R., Babbitt, R., Davies, M., and Hao, W.: Measurements of excess O_3, CO_2, CO, CH_4, C_2H_4, C_2H_2, HCN, NO, NH_3, HCOOH, CH_3COOH, HCHO, and CH_3OH in 1997 Alaskan biomass burning plumes by airborne Fourier transform infrared spectroscopy (AFTIR), J. Geophys. Res., 105, 22147, https://doi.org/10.1029/2000JD900287, 2000.

Graedel, T. and Eisner, T.: Atmospheric formic acid from formicine ants: a preliminary assessment, Tellus B, 40, 335–339, 1988.

Grosjean, D.: Organic acids in southern California air: ambient concentrations, mobile source emissions, in situ formation and removal processes, Environ. Sci. Technol., 23, 1506–1514, 1989.

Grutter, M., Glatthor, N., Stiller, G. P., Fischer, H., Grabowski, U., Höpfner, M., Kellmann, S., Linden, A., and von Clarmann, T.: Global distribution and variability of formic acid as observed by MIPAS-ENVISAT, J. Geophys. Res., 115, D10303, https://doi.org/10.1029/2009JD012980, 2010.

Hatakeyama, S., Washida, N., and Akimoto, H.: Rate constants and mechanisms for the reaction of hydroxyl (OD) radicals with acetylene, propyne, and 2-butyne in air at 297 ± 2 K, J. Phys. Chem., 6, 90, 173–178, 1986.

Hurtmans, D., Coheur, P.-F., Wespes, C., Clarisse, L., Scharf, O., Clerbaux, C., Hadji-Lazaro, J., George, M., and Turquety, S.: FORLI radiative transfer and retrieval code for IASI, J. Quant. Spectrosc. Ra., 113, 1391–1408, https://doi.org/10.1016/j.jqsrt.2012.02.036, 2012.

Hurst, D. F., Griffith, D. W. T., and Cook, G. D.: Trace gas emissions from biomass burning in tropical Australian savannas, J. Geophys. Res., 99, 16441–16456, https://doi.org/10.1029/94JD00670, 1994.

Jacob, D.: Chemistry of OH in remote clouds and its role in the production of formic acid and peroxymonosulfate, J. Geophys. Res., 91, 9807–9826, 1986.

Justice, C. O., Giglio, L., Korontzi, S., Owens, J., Morisette, J. T., Roy, D., Descloitres, J., Alleaume, S., Petitcolin, F., and Kaufman, Y.: The MODIS fire products, Remote Sens. Environ. 83, 244–262, 2002.

Kaskaoutis, D. G., Kumar, S., Sharma, D., Singh, R. P., Kharol, S. K., Sharma, M., Singh, A. K., Singh, S., Singh, A., and Singh, D.: Effects of crop residue burning on aerosol properties, plume characteristics, and long-range transport over northern India, J. Geophys. Res.-Atmos., 119, 5424–5444, https://doi.org/10.1002/2013JD021357, 2014.

Kawamura, K., Ng, L.-L., and Kaplan, I.: Determination of organic acids (C_1–C_{10}) in the atmosphere, motor exhausts, and engine oils, Environ. Sci. Technol., 19, 1082–1086, 1985.

Keene, W. and Galloway, J.: Organic acidity in precipitation of North America, Atmos. Environ., 18, 2491–2497, 1984.

Keene, W. and Galloway, J.: The biogeochemical cycling of formic and acetic acids through the troposphere: An overview of current understanding, Tellus B, 40, 322–334, 1988.

Kerzenmacher, T., Dils, B., Kumps, N., Blumenstock, T., Clerbaux, C., Coheur, P.-F., Demoulin, P., García, O., George, M.,

Griffith, D. W. T., Hase, F., Hadji-Lazaro, J., Hurtmans, D., Jones, N., Mahieu, E., Notholt, J., Paton-Walsh, C., Raffalski, U., Ridder, T., Schneider, M., Servais, C., and De Mazière, M.: Validation of IASI FORLI carbon monoxide retrievals using FTIR data from NDACC, Atmos. Meas. Tech., 5, 2751–2761, https://doi.org/10.5194/amt-5-2751-2012, 2012.

Krol, M., Peters, W., Hooghiemstra, P., George, M., Clerbaux, C., Hurtmans, D., McInerney, D., Sedano, F., Bergamaschi, P., El Hajj, M., Kaiser, J. W., Fisher, D., Yershov, V., and Muller, J.-P.: How much CO was emitted by the 2010 fires around Moscow?, Atmos. Chem. Phys., 13, 4737–4747, https://doi.org/10.5194/acp-13-4737-2013, 2013.

Lee, A., Goldstein, A. H., Kroll, J. H., Ng, N. L., Varutbangkul, V., Flagan, R. C., and Seinfeld, J. H.: Gas-phase products and secondary aerosol yields from the photooxidation of different terpenes, J. Geophys. Res., 111, D17305, https://doi.org/10.1029/2006JD007050, 2006.

Neeb, P., Sauer, F., Horie, O., and Moortgat, G. K.: Formation of hydroxymethyl hydroperoxide and formic acid in alkene ozonolysis in the presence of water vapour, Atmos. Environ., 31, 1417–1423, 1997.

Ohara, T., Akimoto, H., Kurokawa, J., Horii, N., Yamaji, K., Yan, X., and Hayasaka, T.: An Asian emission inventory of anthropogenic emission sources for the period 1980–2020, Atmos. Chem. Phys., 7, 4419–4444, https://doi.org/10.5194/acp-7-4419-2007, 2007.

Ohta, K., Ogawa, H., and Mizuno, T.: Abiological formation of formic acid on rocks in nature, Appl. Geochem., 15, 91–95, 2000.

Paris, J.-D., Ciais, P., Nedelec, P., Ramonet, M., Belan, B. D., Arshinov, M. Yu., Golitsyn, G. S., Granberg, I., Stohl, A., Cayez, G., Athier, G., Boumard, F., and Cousin, J.-M.: The YAK-AEROSIB transcontinental aircraft campaigns: new insights on the transport of CO_2, CO and O_3 across Siberia, Tellus B, 60, 551–568, https://doi.org/10.1111/j.1600-0889.2008.00369.x, 2008.

Paton-Walsh, C., Jones, N. B., Wilson, S. R., Haverd, V., Meier, A., Griffith, D. W. T., and Rinsland, C. P.: Measurements of trace gas emissions from Australian forest fires and correlations with coincident measurements of aerosol optical depth, J. Geophys. Res., 110, D24305, https://doi.org/10.1029/2005JD006202, 2005.

Paulot, F., Wunch, D., Crounse, J. D., Toon, G. C., Millet, D. B., DeCarlo, P. F., Vigouroux, C., Deutscher, N. M., González Abad, G., Notholt, J., Warneke, T., Hannigan, J. W., Warneke, C., de Gouw, J. A., Dunlea, E. J., De Mazière, M., Griffith, D. W. T., Bernath, P., Jimenez, J. L., and Wennberg, P. O.: Importance of secondary sources in the atmospheric budgets of formic and acetic acids, Atmos. Chem. Phys., 11, 1989–2013, https://doi.org/10.5194/acp-11-1989-2011, 2011.

Pochanart, P., Akimoto, H., Kajii, Y., Potemkin, V. M., and Khodzher, T. V.: Regional background ozone and carbon monoxide variations in remote Siberia/East Asia, J. Geophys. Res., 108, 4028, https://doi.org/10.1029/2001JD001412, 2003.

Pommier, M., Law, K. S., Clerbaux, C., Turquety, S., Hurtmans, D., Hadji-Lazaro, J., Coheur, P.-F., Schlager, H., Ancellet, G., Paris, J.-D., Nédélec, P., Diskin, G. S., Podolske, J. R., Holloway, J. S., and Bernath, P.: IASI carbon monoxide validation over the Arctic during POLARCAT spring and summer campaigns, Atmos. Chem. Phys., 10, 10655–10678, https://doi.org/10.5194/acp-10-10655-2010, 2010.

Pommier, M., McLinden, C. A., and Deeter, M.: Relative changes in CO emissions over megacities based on observations from space, Geophys. Res. Lett., 40, 3766–3771, https://doi.org/10.1002/grl.50704, 2013.

Pommier, M., Clerbaux, C., Coheur, P.-F., Mahieu, E., Müller, J.-F., Paton-Walsh, C., Stavrakou, T., and Vigouroux, C.: HCOOH distributions from IASI for 2008–2014: comparison with ground-based FTIR measurements and a global chemistry-transport model, Atmos. Chem. Phys., 16, 8963–8981, https://doi.org/10.5194/acp-16-8963-2016, 2016.

Razavi, A., Karagulian, F., Clarisse, L., Hurtmans, D., Coheur, P. F., Clerbaux, C., M"uller, J. F., and Stavrakou, T.: Global distributions of methanol and formic acid retrieved for the first time from the IASI/MetOp thermal infrared sounder, Atmos. Chem. Phys., 11, 857–872, https://doi.org/10.5194/acp-11-857-2011, 2011.

R'Honi, Y., Clarisse, L., Clerbaux, C., Hurtmans, D., Duflot, V., Turquety, S., Ngadi, Y., and Coheur, P.-F.: Exceptional emissions of NH_3 and HCOOH in the 2010 Russian wildfires, Atmos. Chem. Phys., 13, 4171–4181, https://doi.org/10.5194/acp-13-4171-2013, 2013.

Rinsland, C. P., Boone, C. D., Bernath, P. F., Mahieu, E., Zander, R., Dufour, G., Clerbaux, C., Turquety, S., Chiou, L., McConnell, J. C., Neary, L., and Kaminski, J. W.: First space-based observations of formic acid (HCOOH): Atmospheric Chemistry Experiment austral spring 2004 and 2005 Southern Hemisphere tropical-mid-latitude upper tropospheric measurements, Geophys. Res. Lett., 33, L23804, https://doi.org/10.1029/2006GL027128, 2006.

Rinsland, C. P., Dufour, G., Boone, C. D., Bernath, P. F., Chiou, L., Coheur, P.-F., Turquety, S., and Clerbaux, C.: Satellite boreal measurements over Alaska and Canada during June–July 2004: Simultaneous measurements of upper tropospheric CO, C_2H_6, HCN, CH_3Cl, CH_4, C_2H_2, CH_3OH, HCOOH, OCS, and SF_6 mixing ratios, Global Biogeochem. Cy., 21, GB3008, https://doi.org/10.1029/2006GB002795, 2007.

Rolph, G. D.: Real-time Environmental Applications and Display sYstem (READY) Website, NOAA Air Resources Laboratory, College Park, MD, available at: http://www.ready.noaa.gov (last access: 18 September 2017), 2017.

Rodgers, C. D.: Inverse methods for atmospheric sounding: theory and practice, Ser. Atmos. Ocean. Planet. Phys. 2, World Sci., Hackensack, NJ, 2000.

Sanhueza, E. and Andreae, M.: Emission of formic and acetic acids from tropical savanna soils, Geophys. Res. Lett., 18, 1707–1710, 1991.

Schreier, S. F., Richter, A., Kaiser, J. W., and Burrows, J. P.: The empirical relationship between satellite-derived tropospheric NO_2 and fire radiative power and possible implications for fire emission rates of NO_x, Atmos. Chem. Phys., 14, 2447–2466, https://doi.org/10.5194/acp-14-2447-2014, 2014.

Sinha, P. P., Hobbs, V., Yokelson, R. J., Bertschi, I. T., Blake, D. R., Simpson, I. J., Gao, S., Kirchstetter, T. W., and Novakov, T.: Emissions of trace gases and particles from savanna fires in southern Africa, J. Geophys. Res., 108, 8487, https://doi.org/10.1029/2002JD002325, 2003.

Sinha, P. P., Hobbs, V., Yokelson, R. J., Blake, D. R., Gao, S., and Kirchstetter, T. W.: Emissions from miombo woodland and dambo grassland savanna fires, J. Geophys. Res., 109, D11305, https://doi.org/10.1029/2004JD004521, 2004.

Srinivas, R., Beig, G., and Peshin S. K.: Role of transport in elevated CO levels over Delhi during onset phase of monsoon, Atmos. Environ., 140, 234–241, https://doi.org/10.1016/j.atmosenv.2016.06.003, 2016.

Stavrakou, T., Müller, J.-F., Peeters, J., Razavi, A., Clarisse, L., Clerbaux, C., Coheur, P.-F., Hurtmans, D., and De Mazière, M.: Satellite evidence for a large source of formic acid from boreal and tropical forests, Nat. Geosci., 5, 26–30, https://doi.org/10.1038/ngeo1354, 2012.

Tereszchuk, K. A., González Abad, G., Clerbaux, C., Hurtmans, D., Coheur, P.-F., and Bernath, P. F.: ACE-FTS measurements of trace species in the characterization of biomass burning plumes, Atmos. Chem. Phys., 11, 12169–12179, https://doi.org/10.5194/acp-11-12169-2011, 2011.

Tereszchuk, K. A., González Abad, G., Clerbaux, C., Hadji-Lazaro, J., Hurtmans, D., Coheur, P.-F., and Bernath, P. F.: ACE-FTS observations of pyrogenic trace species in boreal biomass burning plumes during BORTAS, Atmos. Chem. Phys., 13, 4529–4541, https://doi.org/10.5194/acp-13-4529-2013, 2013.

Turquety, S., Hurtmans, D., Hadji-Lazaro, J., Coheur, P.-F., Clerbaux, C., Josset, D., and Tsamalis, C.: Tracking the emission and transport of pollution from wildfires using the IASI CO retrievals: analysis of the summer 2007 Greek fires, Atmos. Chem. Phys., 9, 4897–4913, https://doi.org/10.5194/acp-9-4897-2009, 2009.

Vadrevu, K. P., Lasko, K., Giglio, L., and Justice, C.: Vegetation fires, absorbing aerosols and smoke plume characteristics in diverse biomass burning regions of Asia, Environ. Res. Lett., 10, 2371–2379, https://doi.org/10.1039/c4em00307a, 2015.

van der Werf, G. R., Randerson, J. T., Giglio, L., Collatz, G. J., Mu, M., Kasibhatla, P. S., Morton, D. C., DeFries, R. S., Jin, Y., and van Leeuwen, T. T.: Global fire emissions and the contribution of deforestation, savanna, forest, agricultural, and peat fires (1997–2009), Atmos. Chem. Phys., 10, 11707–11735, https://doi.org/10.5194/acp-10-11707-2010, 2010.

Viatte, C., Strong, K., Hannigan, J., Nussbaumer, E., Emmons, L. K., Conway, S., Paton-Walsh, C., Hartley, J., Benmergui, J., and Lin, J.: Identifying fire plumes in the Arctic with tropospheric FTIR measurements and transport models, Atmos. Chem. Phys., 15, 2227–2246, https://doi.org/10.5194/acp-15-2227-2015, 2015.

Vigouroux, C., Stavrakou, T., Whaley, C., Dils, B., Duflot, V., Hermans, C., Kumps, N., Metzger, J.-M., Scolas, F., Vanhaelewyn, G., Müller, J.-F., Jones, D. B. A., Li, Q., and De Mazière, M.: FTIR time-series of biomass burning products (HCN, C_2H_6, C_2H_2, CH_3OH, and HCOOH) at Reunion Island (21° S, 55° E) and comparisons with model data, Atmos. Chem. Phys., 12, 10367–10385, https://doi.org/10.5194/acp-12-10367-2012, 2012.

Whitburn, S., Van Damme, M., Kaiser, J. W., van der Werf, G. R., Turquety, S., Hurtmans, D., Clarisse, L., Clerbaux, C., and Coheur, P.-F.: Ammonia emissions in tropical biomass burning regions: Comparison between satellite-derived emissions and bottom-up fire inventories, Atmos. Environ, 121, 42–54, https://doi.org/10.1016/j.atmosenv.2015.03.015, 2015.

Whitburn, S., Van Damme, M., Clarisse, L., Hurtmans, D., Clerbaux, C., and Coheur, P.-F.: IASI-derived NH_3 enhancement ratios relative to CO for the tropical biomass burning regions, Atmos. Chem. Phys. Discuss., https://doi.org/10.5194/acp-2017-331, in review, 2017.

White, F.: UNESCO/AETFAT/UNSO vegetation map of Africa, scale 1 : 5,000,000, UNESCO, Paris, 1981.

Wooster, M. J., Roberts, G., Perry, G. L. W., and Kaufman, Y. J.: Retrieval of biomass combustion rates and totals from fire radiative power observations: FRP derivation and calibration relationships between biomass consumption and fire radiative energy release, J. Geophys. Res., 110, D24311, https://doi.org/10.1029/2005JD006318, 2005.

Yokelson, R. J., Bertschi, I. T., Christian, T. J., Hobbs, P. V., Ward, D. E., and Hao, W. M.: Trace gas measurements in nascent, aged, and cloud-processed smoke from African savanna fires by airborne Fourier transform infrared spectroscopy (AFTIR), J. Geophys. Res., 108, 8478, https://doi.org/10.1029/2002JD002322, 2003.

Yokelson, R. J., Karl, T., Artaxo, P., Blake, D. R., Christian, T. J., Griffith, D. W. T., Guenther, A., and Hao, W. M.: The Tropical Forest and Fire Emissions Experiment: overview and airborne fire emission factor measurements, Atmos. Chem. Phys., 7, 5175–5196, https://doi.org/10.5194/acp-7-5175-2007, 2007.

Yokelson, R. J., Christian, T. J., Karl, T. G., and Guenther, A.: The tropical forest and fire emissions experiment: laboratory fire measurements and synthesis of campaign data, Atmos. Chem. Phys., 8, 3509–3527, https://doi.org/10.5194/acp-8-3509-2008, 2008.

Yokelson, R. J., Akagi, S. K., Griffith, D. W. T., and Johnson, T. J.: Interactive comment on "Exceptional emissions of NH_3 and HCOOH in the 2010 Russian wildfires" by Y. R'Honi et al., Atmos. Chem. Phys. Discuss., 12, C11864–C11868, 2013.